UDC 004.855.5(045)
DOI:10.18372/1990-5548.84.20189

[1]V. M. Sineglazov,
[2]K. S. Lesohorskyi

ORTHOPHOTOMOSAICING FRAMEWORK FOR THERMAL AND MULTISPECTRAL IMAGES COLLECTED WITH A UAV FOR INTELLIGENT SYSTEMS

[1]Aviation Computer-Integrated Complexes Department, Faculty of Air Navigation Electronics and Telecommunications, State University "Kyiv Aviation Institute", Kyiv, Ukraine
[2]Faculty of Informatics and Computer Science, National Technical University of Ukraine "Ihor Sikorsky Kyiv Polytechnic Institute," Kyiv, Ukraine

E-mails: [1]svm@nau.edu.ua ORCID 0000-0002-3297-9060,
[2]lesogor.kirill@gmail.com ORCID 0000-0003-2773-7398

***Abstract*—*In this paper, a framework for orthophotomosaicing of multispectral and thermal images collected by unmanned aerial vehicles is presented. The proposed framework is based on a two-stage data preprocessing and mosaicing orthophotographic restoration of images captured with a route-planned unmanned aerial vehicle collection. The super-resolution and image restoration step is handled via a two-pathway U-net image restoration artificial neural network. The framework simplifies the process and makes the collected data less sensitive to noise via image restoration and upscaling steps. The framework was tested on visible, multispectral and thermal images and provides 3.5% and 5.34% improvements in peak signal-to-noise ratio for multispectral and thermal orthophotomosaics.*

Keywords—Machine learning; orthophotomosaicing; image processing; unmanned aerial vehicles; mine detection.

I. INTRODUCTION

Aerial image processing applications have been increasing at a rapid pace with the proliferation of commercially available drones. In the past, to obtain a high resolution aerial imagery, either a plane- or helicopter-based platform had to be used to collect the images, which are costly to operate and maintain. Drones, however, provide a cheap and widespread alternative, allowing for new use cases of aerial imagery.

As such, aerial imagery gained wide adoption in multiple domains – agriculture, environmental surveying, and hazard surveillance. In many of these cases, visible light spectrum cameras are useful, but do not provide information rich enough for a human or an intelligent system to extract features and make decisions. As such, thermal cameras and multi- or hyperspectral cameras are used to provide feature-rich information.

Visible light cameras capture and encode visible light bands as three channels – red, green, and blue. Spectral bands are often blended together to compress information and provide a photorealistic image. This, however, leads to the loss of spectral information, which is necessary for existing spectrometry methods to achieve high accuracy. As such, for specialized applications, multi- and hyperspectral cameras are utilized. Unlike traditional cameras, multi- and hyperspectral cameras capture images as individual spectral bands. In case of multispectral bands, bands are sparse, with 5 to 10 channels being captured across the whole visible light spectrum. Multispectral cameras almost exclusively capture the visible light spectrum, rarely extending into near-infrared or ultraviolet spectrums. Hyperspectral cameras, however, have dense bands, with 100 to 500 channels captured across ultraviolet, visible, and infrared spectra. As such, hyperspectral cameras provide superior spectral information and resolution, but their practical application is limited by their cost and the fact that, in most cases, only certain parts of the spectrum are required.

While multispectral cameras are sufficient if target bands are located in the visible spectrum, some applications necessitate the use of information from the near-infrared spectrum. In such cases, thermal cameras are used. They are more affordable than hyperspectral cameras and provide high-resolution, single-band imagery for the near-infrared spectrum.

As such, multispectral and thermal cameras are the most common choice for outlined applications due to their affordability and providing sufficient information for the majority of use case.

However, unmanned aerial vehicles (UAVs) capture images as a series of individual photos or in a video format. While such a format is sufficient for the object detection task, in various applications, stitching the set of images into a combined area's

birds-eye view scene. This is crucial for semantic segmentation and classification tasks. This process is known as orthophoto mosaic restoration, and comes with a set of challenges. The quality of the restored image can vary greatly, which in turn will have adverse effects on the accuracy of the intelligent systems' training and inference on such data.

This paper aims to provide a comprehensive framework for orthophotomosaic restoration of multispectral and thermal images, while maximizing the quality of the resulting images. The framework includes recommendations for UAV flyby planning, collected image pre-processing algorithms, and orthophoto mosaic restoration algorithms, specifically designed to improve the efficiency of intelligent systems based on computer vision.

II. Literature Review

In this paper, we consider two components of orthophoto mosaic restoration that are crucial for computer-vision-based intelligent systems: individual image pre-processing and orthophoto mosaic stitching.

A. Image preprocessing

Image preprocessing step is designed to enhance the quality of the original image, remove noise, and blur to improve the quality of the restored orthophotomosaic. The image preprocessing step is considered under the setting of image restoration. Image restoration is a fundamental problem in image processing aimed at recovering a clear, pristine image from its degraded version. This degradation often manifests as noise and blur, introduced during image acquisition, transmission, or other environmental factors. The goal is to reverse this degradation process, often formulated as an ill-posed inverse problem, typically represented by the model [1]:

$$g = Hf + n, \quad (1)$$

where g is the observed degraded image, f is the latent original image, H is the degradation operator (e.g., blur kernel), and n is additive noise. The challenge lies in estimating f given g, with partial or no knowledge of H and n.

Image denoising aims to remove unwanted noise while preserving essential image features like edges and textures. Various noise types exist, such as Gaussian, salt-and-pepper, and speckle noise, each requiring tailored approaches.

Spatial filtering algorithms [2] operate directly on image pixels. Examples include mean filters, which smooth images by averaging pixel values in a neighborhood but can blur edges and median filter , which are effective against impulse noise by replacing a pixel with the median value of its neighbors, thereby preserving edges better than mean filters.

Transform domain filtering [3] family of methods transform the image into a different domain, where noise might be more easily separated from the signal. Wavelet denoising leverages the sparsity of image information in the wavelet domain, applying thresholding to wavelet coefficients to suppress noise.

Non-local Means [4] is an advanced filtering technique that exploits the self-similarity of natural images, averaging pixels that have similar neighborhoods, even if they are spatially distant.

More recently, deep learning-based denoising has achieved state-of-the-art results. Convolutional neural networks (CNNs) and transformer-based models learn complex mappings from noisy to clean images, often achieving superior performance by leveraging large datasets [5].

Image deblurring aims to reverse the blurring effect caused by factors like camera motion, object motion, or out-of-focus optics. Deblurring problems are broadly categorized into non-blind and blind deblurring. In the non-blind setting, the blur kernel H is known. Inverse filtering [6] is a direct approach in the frequency domain commonly used for deblurring, but it can amplify noise due to singularities in the blur kernel's frequency response. Wiener filtering minimizes [7] the mean square error between the estimated and original images, considering both the blur kernel and noise statistics. It offers a balance between deblurring and noise suppression. Iterative algorithms like Richardson-Lucy deconvolution [8] or Landweber iteration [9] iteratively refine the estimated image by minimizing a cost function.

In the real world, however, blur kernel H is not known. Such a scenario is more challenging and requires more complex algorithms, often utilizing image priors, such as sparsity and gradient distributions, in combination with regularization techniques. As such, deterministic algorithms underperform when applied to the blind deblurring setting. However, machine learning algorithms are able to efficiently learn the priors, given enough training data. End-to-end CNN [10] architectures in combinations with GANs and visual transformers are used to achieve state-of-the-art deblurring results.

B. Othophotomosaic stitching

Once individual images are processed, the orthophotomosaic scene can be restored. This process involves stitching multiple sub-images to gain optimal seams and assigning a coordinate to

each pixel in the image. More formally, orthophoto mosaicing is a process of generating a continuous, geometrically accurate, and radiometrically consistent image representation of the Earth's surface from multiple individual orthorectified images.

The first step of orthophotomosaic stitching is feature registration. This step ensures that all individual orthophotos are precisely aligned in a common coordinate system. While orthorectification addresses most geometric errors, residual misalignments can persist due to imperfections in the digital elevation model (DEM/DSM), camera calibration, or ground control points (GCPs). Feature-based registration techniques, such as scale-invariant feature transform (SIFT) [11] or speeded up robust features (SURF) [12], are commonly employed to detect and match corresponding points across overlapping images, followed by geometric transformations (e.g., affine, projective, or thin-plate splines) to achieve accurate alignment. Global bundle adjustment techniques are often used to refine the overall block geometry, minimizing cumulative errors.

After the feature extraction step is complete, seamlines between images have to be generated. Seamlines define the boundaries along which individual orthophotos are cut and merged. The objective is to determine optimal paths that minimize radiometric and geometric discontinuities. Ideal seamlines should avoid high-contrast features like building edges, roads, or sharp terrain changes, as these amplify visual artifacts. Several approaches are used for seamline generation. Graph cut [13] algorithms formulate seamline detection as a minimum-cost path problem on a graph, where nodes represent pixels and edge weights represent the cost of cutting through that pixel. This allows for globally optimal seamlines, but such algorithms are computationally intensive. Voronoi diagrams can be used to define boundaries equidistant from image centers, though they may cut through critical features. Variants like "area Voronoi diagrams with overlap" improve upon this. Feature-based seamline algorithms follow low-gradient areas or exploit object boundaries to ensure that objects are not cut awkwardly.

Radiometric calibrations [14] is the final step of orthophoto mosaic stitching that aims to smooth artifacts and subtle differences along the seamlines to improve the alignment of the resulting orthophoto mosaic. During this step, four transformations are performed: histogram matching, alpha blending, global radiometric adjustment, and shadow and illumination correction.

Histogram matching rebalances the radiometric properties, such as brightness and contrast, of individual images to either a common reference or a global average of multiple images. This ensures even data distribution, which makes the resulting orthophotomosaic easier to process both visually and computationally. Alpha blending applies weighted averaging of pixel values in the regions with identified overlap with varying linear and non linear weights across the seamline to create a more gradual transition. Global radiometric calibration is applied to the entire orthophoto mosaic, rather than individual patches, and uses statistical analysis of overlapping regions to minimize artifacts across the entire mosaic. Lastly, shadow and illumination correction addresses varying illumination conditions and project shadows to achieve a more uniform appearance.

While the approach to orthophotomosaic restoration is well developed, some of the challenges still remain. Firstly, geometry artefacts are common around tall structures, where even orthorectification cannot entirely eliminate radial displacement from oblique views. Secondly, when images are acquired under varying atmospheric or illumination conditions, radiometric inconsistencies are prominent and decrease the overall quality of the image. Lastly, processing large datasets of high-resolution imagery for seamless mosaicking can be computationally intensive.

Recent advancements, particularly driven by deep learning, are addressing these challenges. Neural networks, specifically convolutional neural networks and visual transformers, are used in the image stitching pipeline to address the challenges outlined above. Machine-learning-based methods have several advantages, namely:

- *enhanced feature matching* by learning robust features for registration in challenging scenarios;
- *automated and optimized seamline detection* – deep learning models can learn to identify optimal seamlines that minimize visual artifacts and respect semantic object boundaries more effectively than traditional cost functions;
- *seamless radiometric harmonization* – end-to-end learning approaches that implicitly learn radiometric transformations to produce highly seamless mosaics without explicit blending parameters;
- *true orthophoto generation* – deep learning aids in inferring 3D structures and identifying occluded areas for more accurate true orthophoto mosaics.

III. Problem Statement

More formally, the process of orthomosaic restoration is defined as a transformation of the input

image set I_n into an orthophotomosaic O. Each image in the set I_n is defined as an 3-dimensional tensor $I: I \times \mathbb{R}^{H \times W \times C}$, where H is the height of the image, W is the width of the image and C is the number of channels. Orthophotomosaic is defined as a 3-dimensional tensor $O: O \in \mathbb{R}^{H' \times W \times C}$, where H' and W' are the height and width dimensions of the orthophotomosaic. It is worth noting that for the input set, all of the images share dimensions H, W, and C. In the orthophoto, W' and H' depend on the reconstruction results and are not known ahead of time, but can be no less than the singular image dimensions $H' >= H$, $W' >= W$. The number of channels C is shared across both the input image set I_n and the orthophoto O.

The process of end-to-end photomosaic is defined as a mapping between the input image space I_n and the corresponding reconstructed orthophotomosaic O:

$$O = f(I_n, \theta), \tag{2}$$

here O is the reconstructed orthophotomosaic; I_n is the input image and θ are reconstruction parameters – either learnt through machine learning or defined empirically.

In this work, the restoration process is defined as a composition of multiple steps of the processing pipeline.

To evaluate the efficiency of the pipeline, the peak signal-to-noise ratio (PSNR) metric is used. While not a perfect estimate of the seam quality, it is crucial for intelligent system processing. Peak signal-to-noise ratio is defined as:

$$\text{PSNR} = \frac{1}{HW} \sum_{i=0}^{W} \sum_{j=0}^{H} \left[I(i,j,c) - K(i,j,c) \right]^2, \tag{3}$$

where $I(i, j, c)$ is the value of i, j pixels's channel c, $K(i, j, c)$ is the maximum possible strength for the signal in the given band.

IV. METHOD

The proposed method consists of two steps: individual image preprocessing and orthophotomosaic stitching. Image pre-processing utilizes a scalable pre-trained U-net-based neural network to improve the source dataset quality. The orthophotomosaic stitching is based on the set of feature-based deterministic rectification, extraction and stitching algorithms.

A. Data Preprocessing

Data preprocessing step aims to improve the quality of the orthomosaic O by improving the quality of individual images. The methodology is based on the iteration of the authors' previous work [15], adapted for use without a receptive window. The network architecture is also modified to be more efficient, as can be seen in Fig. 1.

The neural network is pre-trained on the vast dataset for image reconstruction tasks, and is then fine-tuned on the images from the input set I_n. The training process is based on supervised learning from the augmented images. The synthetic degradation operator follows the general form outlined in (1) and is a composition of noise and blur applied to the source image. In this research, channel-aware noise models and uniform noise kernels are used.

Channel-aware noise is modeled as a three dimensional Gaussian noise with a random center:

$$G(x,y,z) = \frac{e^{\frac{(x-x')^2+(y-y')^2+(z-z')^2}{2\sigma^2}}}{2\pi^{3/2}\sigma^3}, \tag{4}$$

where σ is the deviation parameter of the distribution and controls the "strength" of the noise, x', y', z' are the centre coordinates of the noise, x, y, z are the coordinates of the current pixel. The noise is introduced in a random centre x', y', z' drawn from a uniform discrete distribution.

This model captures the fact that certain channels, especially in multispectral / hyperspectral images are more affected by noise than others.

In case of thermal imagery and as a blur model, a two-dimensional variation of the gaussian kernel are used:

$$G(x,y) = \frac{e^{\frac{(x-x')^2+(y-y')^2}{2\sigma^2}}}{2\pi\sigma^2}, \tag{5}$$

where σ is the deviation parameter of the distribution and controls the "strength" of the noise, x', y' are the centre coordinates of the noise, x, y, are the coordinates of the current pixel. The noise is introduced in a random centre x', y' drawn from a uniform discrete distribution.

In addition to Gaussian blur, motion blur is simulated as a most likely type of noise in the UAV-based video capture. It is emulated by applying the one-hot encoded blur kernel initialized with the random value drawn from a normal distribution (5) with σ = 0.5. This emulates the strength of motion blur, but also ensures that overall impact of blur is limited. The final step of blur kernel formation is to rotate it to simulate the movement in different

direction. To achieve this, an Euclidian rotation is used:

$$Rv = \begin{bmatrix} x\cos x\cos\theta - y\sin\theta \\ x\sin\theta + y\cos\theta \end{bmatrix}, \quad (6)$$

where θ is the rotation degree, *x, y* are coordinates of the pixel.

The blur is applied across all channels, simplifying the application of the filters. The scheme outlined above ensures that blur strength can be controlled to create varied augmentations.

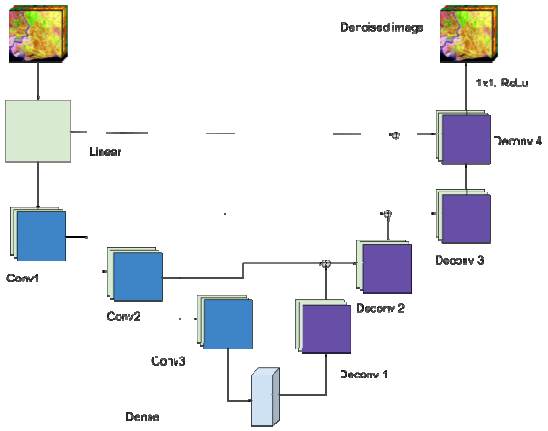

Fig. 1. Neural network architecture

The network architecture is a variation of a U-Net. Unlike previous work, the framework was switched from the iterative residual reconstruction to one-shot reconstruction, as images collected for orthomosaics usually have less noise in comparison to other types of fly-bys. The network consists of three constriction bottlenecks, feature extraction dense layers and three deconvolution bottlenecks. Constriction bottleneck consists of two convolutional layers and one ReLu activation layer. Deconvolutional layer adds one deconvolution operation after ReLu, but otherwise follows the same architecture. Residual connections are present to pass original image information to both the deconvolution pathway.

B. Orthophotomosaic stitching

Orthophotomosaic stitching step consists of 6 substeps:

1) lens distortion correction. During this step, images are corrected using camera lens information, if available;

2) structure from motion for sparse point cloud generation. A state from motion algorithm is used to identify common features across overlapping images. This information is used to compute the relative position of each camera in 3D position and form geometric alignment between shots;

3) multi-view stereo dense point cloud generation. This step utilizes sparse point cloud and camera poses, a 2.5D dense point cloud is generated. The density and accuracy of this point cloud are crucial for subsequent orthorectification, as it serves as the Digital Surface Model (DSM);

4) orthorectification. This step removes perspective distortions by utilizing estimated camera positions and DSM to map each individual pixel to ground coordinates, which is used to correct geometric degradations;

5) seamline generation. Seamline is generated for the orthorectified images by using a min-cut graph algorithms to select stitching that minimizes the gradient of the seamline;

6) radiometric blending addresses radiometric inconsistencies (brightness/color variations) between individual orthophotos. This can involves histogram matching, local adjustments, or feathering/blending algorithms that create a smooth transition across the chosen seamlines. The goal is to achieve a uniform appearance across the entire mosaic, mitigating "patchiness".

The final step of the processing involves the stitching of orthorectified images along the identified seamline.

The process is complex and while neural networks could be applied for i.e. seamline identification, they would require fine tuning on the target dataset to yield adequate results. Unlike individual image preprocessing, however, they require explicitly labeled pairs of samples and cannot require on priors as it is done in the individual image reconstruction. As such, neural networks yield subpar results comparable to deterministic algorithms, and are ill suited for this problem under considered setting.

Considering this, a set of deterministic algorithms is used. This work uses an opensource orthophoto mosaicing pipeline – OpenDronMap (ODM) [16] with planar orthorectification for image processing.

B. Programmatic implementation

The preprocessing pipeline is implemented as a python library. The pipeline is wrapped into a docker container based on OpenDronMap's open-source docker container. The data is provided via docker volumes.

The docker image executes in stages and includes a parameter preset for ODM processing, which can be overridden by passing appropriate flags to the docker command.

Lastly, each step of the pipeline includes checkpointing and persistent storage of the stage

results, which enables data re-usage between stages and a failsafe in case of partial stage failures. The full diagram of the process is demonstrated in Fig. 2.

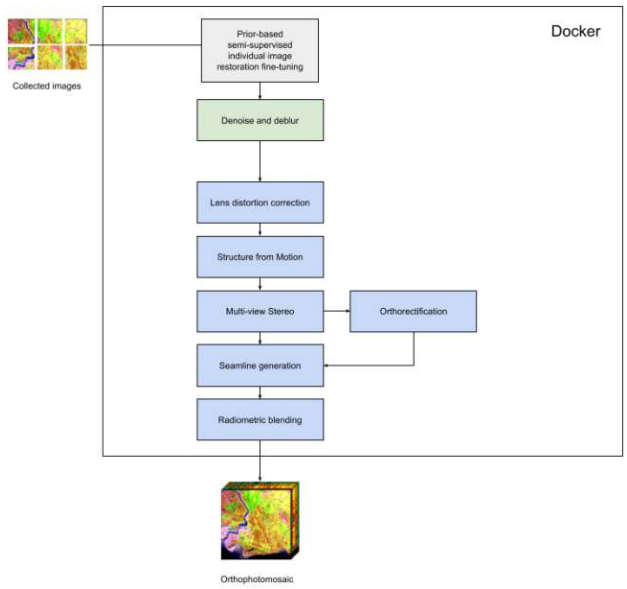

Fig. 2. Orthophotomosaic Stitching Pipeline Diagram

V. Experiment and Results

To verify the approach a controlled experiment on multispectral and thermal data was performed. The datasets are proprietary and were captured over a field using two different types of UAVs and cameras, however the flybies were performed at the same height and covered the same area.

The thermal dataset consists of 456 images captured at 12 meters. The multispectral dataset is smaller and contains 232 images captured at 15 meters. One of the reasons for such a discrepancy is low field of view of the thermal camera.

The proposed pipeline was applied to each dataset individually. In the first run, the pre-processing step is skipped and orthophotomosaic is restored independently, which serves as a baseline. The second run is performed 5 times, during which a pre-processing network is trained and applied to the input images. Pre-processing network is pre trained using the Indian Pines and Pavia University datasets.

The following hyperparameters are used: learning rate of 0.001, optimizer is Adam, noise kernels use medium noise configuration ($\sigma = 0.3$), auto-boundary for ODM is set to true, and sfm-algorithm is planar.

To evaluate the results, PSNR metric is used. Additionally, the individual average peak signal to noise ratio (IAPSNR) is calculated to measure the quality of both orthophotomosaic and individual images. The experimental results are given in Table I.

TABLE I. Orthophotomosaicing Results

Dataset	PSNR	IAPSNR
Multispectral (no pre-processing)	33.08	31.52
Multipsectral	34.21	32.034
Thermal (no pre-processing)	42.253	39.251
Thermal	44.513	42.521

The examples of stitched orthophotomosaics are given on the right.

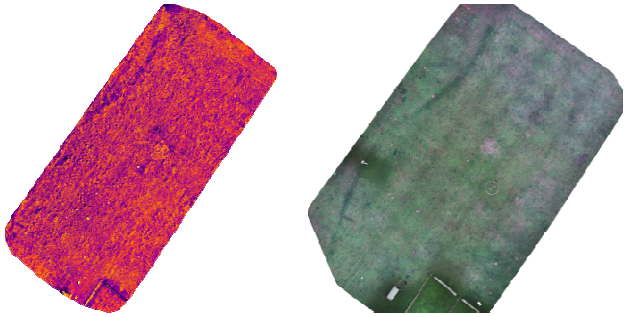

Fig. 3. Examples of the restored orthophotomosaics – thermal (left) and multispectral (right)

The proposed method is efficient in the reconstruction of orthohpotomosaics, however visually it is harder to identify the effect of the proposed method. Pre-processing step provides an increase in PSNR of 3.5% for multispectral and 5.34% for thermal datasets, which is significant for machine learning models which use the stitched orthophotos for decision making. The proposed pipeline includes multiple steps that are utilized during the image preprocessing, thus making the data useful for intelligent systems.

VI. Conclusion

The proposed orthophotomosaic reconstruction pipeline is capable of restoring orthophotomosaics. The proposed method is scalable and can be parallelized by leveraging distributed computations. The introduction of pre-processing step improves the quality of orthophotomosaic by 5.34% and 3.5% on the thermal and multispectral datasets used for testing.

However, as noted above, the visual quality of the restored orthophoto mosaic remains approximately the same, with some artifacts introduced along the seams during the stitching process.

Future work entails the improvement of a orthophotomosaic post-processing step to reduce the number of artifacts along the seam lines. Additional metrics to objectively assess the visual quality of image must be used to determine the modification's efficiency.

REFERENCES

[1] P. Bergmans, “A simple converse for broadcast channels with additive white gaussian noise (corresp.),” IEEE Trans. on Information Theory, 1974, vol. 20, no. 2, pp. 279-280. https://doi.org/10.1109/TIT.1974.1055184

[2] Wong, Chi Man, et al. "Spatial filtering in SSVEP-based BCIs: Unified framework and new improvements." IEEE Transactions on Biomedical Engineering 67.11 (2020): 3057-3072. https://doi.org/10.1109/TBME.2020.2975552

[3] Roy, Vandana, and Shailja Shukla. "Spatial and transform domain filtering method for image de-noising: a review." International Journal of Modern Education and Computer Science 5.7 (2013): 41. https://doi.org/10.5815/ijmecs.2013.07.05

[4] Buades, Antoni, Bartomeu Coll, and Jean-Michel Morel. "Non-local means denoising." Image Processing On Line 1 (2011): 208-212. https://doi.org/10.5201/ipol.2011.bcm_nlm

[5] Liu, Zhe, Wei Qi Yan, and Mee Loong Yang. "Image denoising based on a CNN model." 2018 4th International conference on control, automation and robotics (ICCAR). IEEE, 2018. https://doi.org/10.1109/ICCAR.2018.8384706

[6] Michailovich, Oleg, and Allen Tannenbaum. "Blind deconvolution of medical ultrasound images: A parametric inverse filtering approach." IEEE Transactions on Image Processing 16.12 (2007): 3005-3019. https://doi.org/10.1109/TIP.2007.910179

[7] Robinson, Enders A., and Sven Treitel. "Principles of digital Wiener filtering." Geophysical Prospecting 15.3 (1967): 311-332. https://doi.org/10.1111/j.1365-2478.1967.tb01793.x

[8] Ingaramo, Maria, et al. "Richardson–Lucy deconvolution as a general tool for combining images with complementary strengths." ChemPhysChem 15.4 (2014): 794-800. https://doi.org/10.1002/cphc.201300831

[9] Real, Rommel, and Qinian Jin. "A revisit on Landweber iteration." Inverse problems 36.7 (2020): 075011. https://doi.org/10.1088/1361-6420/ab8bc4

[10] Min, Chao, et al. "Blind deblurring via a novel recursive deep CNN improved by wavelet transform." IEEE Access 6 (2018): 69242-69252. https://doi.org/10.1109/ACCESS.2018.2880279

[11] Lindeberg, Tony. "Scale invariant feature transform." (2012): 10491. https://doi.org/10.4249/scholarpedia.10491

[12] Bay, Herbert, et al. "Speeded-up robust features (SURF)." Computer vision and image understanding 110.3 (2008): 346-359. https://doi.org/10.1016/j.cviu.2007.09.014

[13] Peng, Zongyi, et al. "Seamless UAV hyperspectral image stitching using optimal seamline detection via graph cuts." IEEE Transactions on Geoscience and Remote Sensing 61 (2023): 1-13. https://doi.org/10.1109/TGRS.2023.3275970

[14] Wyatt, Clair. Radiometric calibration: theory and methods. Elsevier, 2012.

[15] Sineglazov, Viktor, Kyrylo Lesohorskyi, and Olena Chumachenko. "Faster Image Deblurring for Unmanned Aerial Vehicles." 2024 2nd International Conference on Unmanned Vehicle Systems-Oman (UVS). IEEE, 2024. https://doi.org/10.1109/UVS59630.2024.10467152

[16] Glossner, John, Samantha Murphy, and Daniel Iancu. "An overview of the drone open-source ecosystem." arXiv preprint arXiv:2110.02260 (2021).

Received February 17, 2025

Sineglazov Victor. ORCID 0000-0002-3297-9060. Doctor of Engineering Science. Professor. Head of the Department.
Aviation Computer-Integrated Complexes Department, Faculty of Air Navigation Electronics and Telecommunications, State University “Kyiv Aviation Institute”, Kyiv, Ukraine.
Education: Kyiv Polytechnic Institute, Kyiv, Ukraine, (1973).
Research area: Air Navigation, Air Traffic Control, Identification of Complex Systems, Wind/Solar power plant, artificial intelligence.
Publications: more than 670 papers.
E-mail: svm@nau.edu.ua

Lesohorskyi Kyrylo. ORCID 0000-0002-3297-9060. PhD Student.
Department of Information Systems, Faculty of Informatics and Computer Science, National Technical University of Ukraine "Igor Sikorsky Kyiv Polytechnic Institute", Kyiv, Ukraine.
Education: National Technical University of Ukraine "Igor Sikorsky Kyiv Polytechnic Institute", Kyiv, Ukraine, (2022).
Research interests: artificial neural networks, artificial intelligence, distributed computing.
Publications: 18
E-mail: lesogor.kirill@gmail.com

В. М. Синєглазов, К. С. Лесогорський. Фреймворк для побудови ортофотоплану термальних та мультиспектральних зображень отриманих із БПЛА для інтелектуальних систем
У статті представлено фреймворк для ортофотомозаїки мультиспектральних та теплових зображень, зібраних безпілотними літальними апаратами. Запропонований фреймворк базується на двоетапній попередній обробці даних та мозаїчному ортофотографічному відновленні зображень, отриманих за допомогою маршрутно спланованої колекції безпілотних літальних апаратів. Етап надвисокої роздільної здатності та відновлення зображень виконується за допомогою двоканальної штучної нейронної мережі для відновлення зображень U-net. Фреймворк спрощує процес і робить зібрані дані менш чутливими до шуму завдяки етапам відновлення зображення та масштабування. Фреймворк був протестований на видимих, мультиспектральних та теплових зображеннях і забезпечує покращення пікового співвідношення сигнал/шум на 3,5% та 5,34% для мультиспектральних та теплових ортофотомозаїк.
Ключові слова: машинне навчання; ортофотоплан; обробка зображень; безпілотні літальні апарати; виявлення мін.

Синєглазов Віктор Михайлович. ORCID 0000-0002-3297-9060. Доктор технічних наук. Професор. Завідувач кафедри авіаційних комп'ютерно-інтегрованих комплексів. Факультет аеронавігації, електроніки і телекомунікацій, Державний університет «Київський авіаційний інститут», Київ, Україна.
Освіта: Київський політехнічний інститут, Київ, Україна, (1973).
Напрям наукової діяльності: аеронавігація, управління повітряним рухом, ідентифікація складних систем, вітроенергетичні установки, штучний інтелект.
Кількість публікацій: більше 670 наукових робіт.
E-mail: svm@nau.edu.ua

Лесогорський Кирило Сергійович. ORCID 0000-0003-2773-7398. Аспірант.
Кафедра штучного інтелекту, Інститут прикладного системного аналізу, Національний технічний університет Україні «Київський Політехнічний Інститут імені Ігоря Сікорського», Київ, Україна.
Освіта: Національний технічний університет Україні «Київський політехнічний інститут імені Ігоря Сікорського», (2022).
Напрям наукової діяльності: штучні нейронні мережі, штучний інтелект, розподіленні обчислення.
Кількість публікацій: 18.
E-mail: lesogor.kirill@gmail.com